Molecular Crystals and Liquid Crystals Science and Technology. Section A. Molecular Crystals and Liquid Crystals

Publication details, including instructions for authors and subscription information:
http://www.tandfonline.com/loi/gmcl19

Formation Mechanism of Polymeric Fullerenes

Y. Iwasa [a] , T. Ozaki [a] & T. Mitani [a]

[a] Japan Advanced Institute of Science and Technology Tatsunokuchi, Ishikawa, 923-1292, Japan

Version of record first published: 24 Sep 2006

To cite this article: Y. Iwasa, T. Ozaki & T. Mitani (2001): Formation Mechanism of Polymeric Fullerenes, Molecular Crystals and Liquid Crystals Science and Technology. Section A. Molecular Crystals and Liquid Crystals, 355:1, 445-456

To link to this article: http://dx.doi.org/10.1080/10587250108023676

Mol. Cryst. Liq. Cryst., Vol. 355, pp. 445-456
Reprints available directly from the publisher
Photocopying permitted by license only

Formation Mechanism of Polymeric Fullerenes

Y. IWASA, T. OZAKI and T. MITANI*

Japan Advanced Institute of Science and Technology Tatsunokuchi, Ishikawa 923–1292, Japan

(Received October 12, 1999; In final form January 18, 2000)

The energetics and reaction paths of polymeric forms of fullerenes have been investigated by means of calorimetry experiment and semiempirical molecular orbital calculations. Energy schemes of three types of single phase C_{60} polymers *i.e.*, dimer, one- and two-dimensional polymers have been experimentally established. This energy scheme, as well as the dramatic difference in experimental conditions for the polymerization and the depolymerization, is reasonably explained by a calculated energy contour map taking the distortion of fullerene molecules into account.

Keywords: polymeric fullerenes; thermal stability; intrinsic reaction coordinates

I. INTRODUCTION

Fullerene is a kind of cluster composed mainly of carbon. Among them, C_{60} is the most well known due to its characteristic soccer ball shape and its abundance. Fullerene clusters were first predicted theoretically by Osawa in 1970 [1], and experimentally found by Kroto, Smalley and coworkers in 1985 [2]. Although the work on fullerenes in the 1980's was limited to gas-phase experiments and theoretical calculations, the discovery in 1990 by Krätchmer *et al.* of a simple and inexpensive method to produce large quantities of fullerene clusters [3] provided a great stimulus to the research filed of fullerenes. Interestingly, these experimental breakthroughs have been made by astrophysicists, not by materials scientists. This interdisciplinary nature is a unique and attractive aspect of fullerene research.

* Corresponding Author.

Immediately after the discovery of Krätchmer method, intercalation of alkali metals into fullerene solids was found to afford a new type of conductor, the first three-dimensional molecular conductor [4]. Hebard *et al.* cooled down the potassium doped C_{60} samples measuring resistivity and magnetization, both of which showed unambiguous evidence for bulk superconductivity with the onset temperature at 19K [5]. These findings of intercalation and superconductivity have triggered a fever of fullerene research.

Later in 1993, another unique aspect of solid state fullerenes has been discovered: That is the polymerization of fullerenes. Rao *et al.* found that the light irradiation on the undoped films of C_{60} causes the polymerization [6]. They proposed a [2+2] cycloaddition as a possible interfullerene bonding. However, since the photo-induced polymerization did not occur coherently throughout the crystal, the polymerized product has been obtained as noncrystalline materials. Thus the nature of interfullerene bonds was unclear in 1993. In 1994, two alternative routes to promote fullerene polymerization have been found almost simultaneously. Slow cooling of alkali metal intercalated C_{60} compounds was found to induce a spontaneous polymerization of C_{60} [7]. Another method is the high pressure/high temperature treatment of undoped C_{60} solids [8]. These two methods yielded doped and undoped polymers, respectively. The importance of these findings is that obtained polymers are crystalline materials which enable researchers to investigate detailed structure and properties of polymerized fullerenes. Figure 1 shows three types of neutral fullerene polymers produced by a high pressure synthesis technique. In this paper, we discuss on the energetics and formation mechanisms of neutral fullerene polymers.

II. EXPERIMETAL DETERMINATION OF ENERGETICS OF POLYMERIZED FULLERITES

In the undoped (neutral) polymers, the intermolecular bonds are [2+2] cycloadditions, and various polymer networks can be obtained by changing their synthesis conditions. After the discovery of the 2D rhombohedral polymer [8], three types of polymers have been identified [9]. Subsequently, the synthesis conditions on the pressure-temperature plane have been clarified [10], followed by an improvement of crystallinity in the 1D polymer [11,12]. Meanwhile, a mechanochemical reaction succeeded in producing C_{60} dumbbell dimers [13]. A variety of neutral polymers means that pure solid carbon has several metastable phases near fullerenes. This phenomenon is another unique aspect of solid state fullerenes, reflecting the flexible character of sp^2/sp^3 carbon. Moreover, the conversions occurring

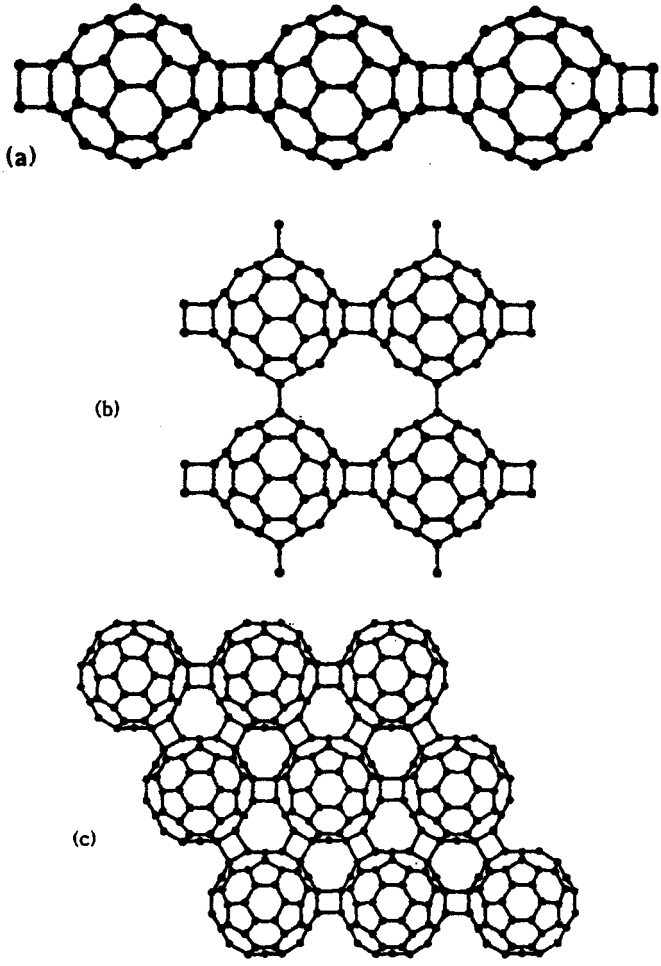

FIGURE 1 Three types of neutral (undoped) polymeric fullerenes. (a) 1D-orthorhombic, (b) 2D-tetragonal, and (c) 2D-rhombohedral polymers, synthesized by high pressure technique

at moderate temperatures suggest that these polymeric phases compete in a small energy scale.

Here we focus on the energetics of three types of polymerized fullerites; dimer, 1D- and 2D-rhombohedral polymers. High pressure synthesis of these polymers was carried out using a cubic anvil high pressure apparatus as described in literatures [8,9,11,14]. Phase purity was monitored by x-ray diffraction patterns and infrared absorption spectra. Both experiments showed that the dimer and 2D-pol-

ymer phases were in single phase with rather high quality, while the quality of the 1D polymer sample is relatively poor. The infrared mode assignment is being carried out in terms of the group theory [15,16].

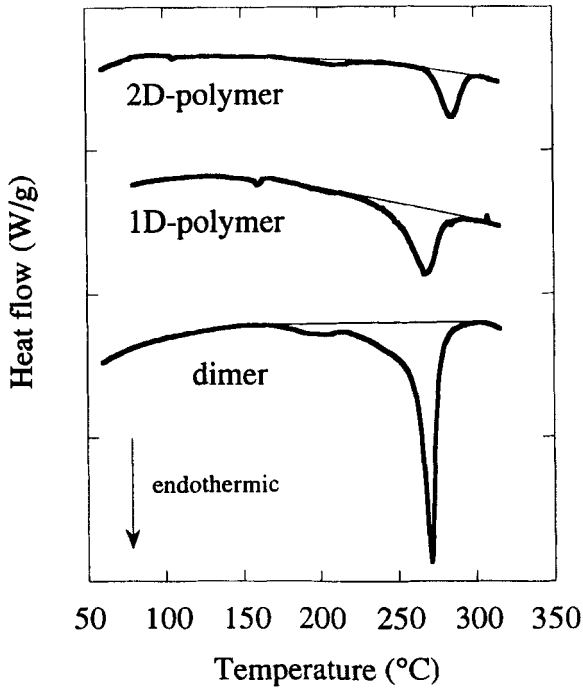

FIGURE 2 Differential scanning calorimetry data for the dimer, 1D-polymer, and 2D-rhombohedral polymer in the heating process of which the heating rate was 10°C/min. The thick solid lines are experimental data and thin lines display the background assumed when calculating the enthalpy change ΔH. All these materials revert to monomer C_{60} after the DSC measurement

These polymeric forms are stable in the ambient conditions (room temperature and ambient pressure). However, all these materials commonly revert back to the monomeric C_{60} by heating at ambient pressure [17]. A differential scanning calorimetry (DSC) measurement was made on 10–15mg powder samples each using a commercial calorimeter. Figure 2 shows DSC data for C_{60} dimer, 1D-polymer, and 2D-rhombohedral polymers in the heating process at a heating rate of 10°C/min. We found a large endothermic peak in the heating process, but no signal was observed in the cooling scan, indicating that an irreversible transition occurred in the heating process. The substances obtained after the DSC measurements were all monomer C_{60} as confirmed by infrared and x-ray diffraction measurements. These data clearly showed that all polymeric forms of C_{60}

revert to monomers upon heating to 300°C. This conversion takes place as an endothermic reaction, indicating that all the polymeric forms are energetically stable compared to the monomer.

The area of the peak in the DSC data (Fig. 2) is identical to the enthalpy change ΔH. The assumed background is shown by thin solid lines. Since the volume change associated with the bond breaking is extremely small, the enthalpy change ΔH directly corresponds to the change of internal energy: $\Delta H = -E$, where E is the energy of the polymeric C_{60} measured from that of the monomeric fcc phase at the bond-breaking temperature. Figure 3 summarizes the relation between E and the number of [2+2] bonds per C_{60}. Here the dimer, one- and two-dimensional polymers contains one, two, and six intermolecular [2+2] bonds per molecule. The negative E values mean that the polymeric phases are more stable than the monomeric phase.

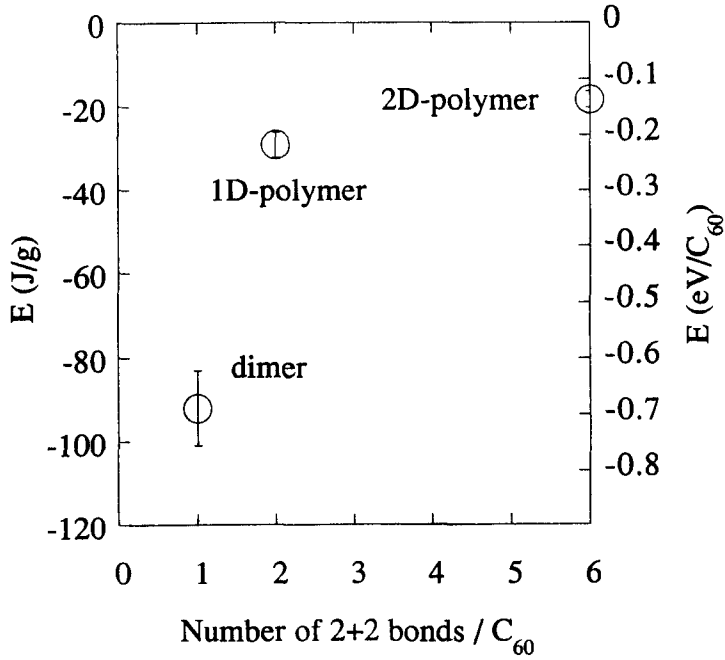

FIGURE 3 The relative energy of the C_{60} dimer, 1D-orthorhombic, and 2D-rhombohedral polymers measured from the energy of monomeric fcc C_{60}, plotted as a function of the number of [2+2] intermolecular bonds per C_{60} molecule

The vertical axis in Fig. 3 is shown in units of J/g and eV/ C_{60}, for left and right side, respectively. It is noted that the energy difference between the mono-

mer and dimer is about 0.69 eV/ C_{60} or 0.011 eV/C atom. The E value derived from the DSC measurement is the difference in the energy minima of the dimeric and monomeric phases. On the other hand, the energy barrier for the depolymerization process from dimers to monomers has been obtained to be 1.75eV by a high resolution capacitance dilatometry measurement by Nagel *et al.* [18]. Figure 4 displays a speculative energy diagram for the relation between the monomeric and dimeric phases, constructed from the two experimental observations. Interestingly, the conversion from the less stable monomer phase requires a hard condition such as high pressure/high temperature or light irradiation, while the reverse reaction from the more stable polymer phase to the monomer phase occurs under milder conditions. This energy scheme is discussed theoretically in the following section.

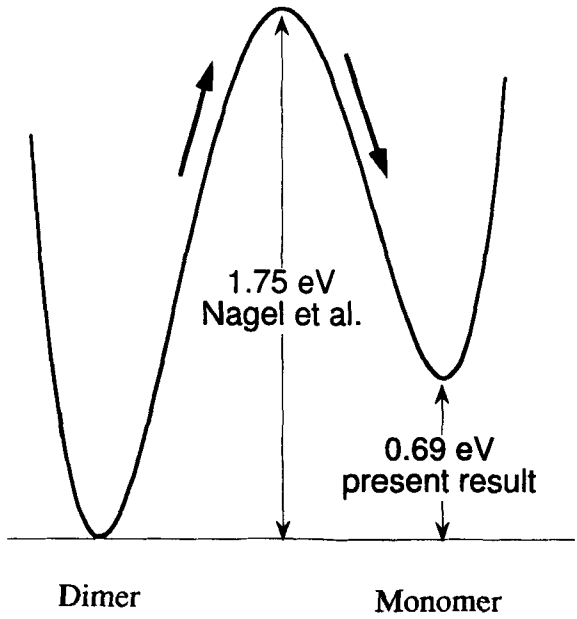

FIGURE 4 Schematic energy diagram of the dimeric and monomeric C_{60} derived from the experimental results on the bond-breaking process

Another indication of Fig. 3 is that the energy of the polymeric phases becomes higher when the number of [2+2] bonds increases. Since the polymeric phases are stabilized by the formation of intermolecular bonds, the polymers are expected to be more stable in energy as the number of the bonds increases. The unexpected trend in Fig. 3 is explained as follows: In the polymeric forms, one

should consider both the energy gain due to the bond formation and energy loss due to the molecular deformation. Since the former contribution dominates, the polymeric forms become lower in energy than the monomer phase. However, the intermolecular bond causes a significant deformation of the C_{60} cage. The deformation energy is able to be absorbed by the intramolecular relaxation in the dimer case. As the number of intermolecular bonds increases, the molecular deformation increases significantly and the stabilization by bond formation is less effective than that of the dimer case. This deformation energy cancels the energy gain by bond formation, so that the energy of polymers increases with the number of the [2+2] bonds. This scenario may explain the trend shown in Fig. 3.

III. CALCULATION OF REACTION PATHS AND POTENTIALS

To explain the energy diagram in Fig. 4 and to clarify the contrasting behaviors of dimerization and decomposition processes, we calculated an energy contour map and intrinsic reaction coordinates (IRC), in the framework of semiempirical molecular orbital calculation, in terms of the intermolecular distance $q_1$and the intramolecular distortions q_2 [19]. The energy of a distorted C_{60} pair was determined by a geometry optimization with a constraint. The constraint was given by fixing eight atoms in a C_{60} pair, where the C_{60} pair has two pairs of parallel 6/6 bonds between two C_{60} molecules, and the fixed eight atoms constructs these four 6/6 bonds. Within this constraint, the geometry of the distorted C_{60} pair was optimized keeping the distance between the centers of mass in the pair and a degree of distortion constant. We obtained the energy contour map shown in Fig. 5, by applying the geometry optimization with the above constraint for the C_{60} pair. Here q_1 is the distance between the centers of mass of two C_{60}molecules, and q_2 is the difference between the distorted C_{60} molecule (d') and I_h C_{60} (d) in diameter, i.e. $q_2 = d'-d$. Thus, positive q_2 means elongation of the molecule, while negative q_2 means compression. The left and right sides in Fig. 5 correspond to the intermolecular bonding dimer state and the non-bonding monomer state, respectively.

We calculated intrinsic reaction coordinates [20] on the energy contour map, using an external force (IRC-EF) which is equivalent to pressure. Although this calculation was performed within a C_{60} pair model, it enables us to elucidate the role of molecular distortion of C_{60} in the polymerization and depolymerization in solid state. The following equations are derived by introducing pressure in the general IRC formulation:

$$\frac{dq_1}{ds} = \left(\frac{\partial W}{\partial q_1} + p\right) \Big/ \frac{\partial W}{\partial s} \tag{1}$$

$$\frac{dq_2}{ds} = \frac{\partial W}{\partial q_2} \Big/ \frac{\partial W}{\partial s} \tag{2}$$

$$\frac{\partial W}{\partial s} = -\left[\left(\frac{\partial W}{\partial q_1} + p\right)^2 + \left(\frac{\partial W}{\partial q_2}\right)^2\right]^{1/2} \tag{3}$$

where W is the potential energy, and s is equivalent to the total reaction path. p is the external force corresponding to pressure and is a constant value acting toward the negative direction of the $q_1$axis. Since the external pressure can not elongate a C_{60} molecule, the q_2 element of the external pressure p should not be positive. Here the q_2 element of the external force $p$is assumed to be zero.

The IRC-EF is shown as a thin solid line in Fig. 5, where p is 13 eV/Å. The early path proceeds in the direction belong to the q_1 axis due to action of the external force. In other words, the external force moves two C_{60} molecules toward each other, without significant deformation of the molecules. Then the internal stress deforms the C_{60} molecules pushing the reaction path to the negative q_2 side, resulting in a molecular warping. Eventually, the IRC-EF reaches the seam, and when it goes over the seam the intermolecular bonds are formed. Then, the path of the C_{60} molecules reaches a dead end at the point where the internal stress balances the external force. At this point we release the external force, followed by a relaxation of the C_{60} pair into the stable dimer point.

This model calculation suggests that the activation energy in the polymerization under high-pressure becomes large as a result of the distortion of a C_{60} molecule. In a usual chemical reaction, the expected IRC follows a line with the lowest activation energy. Actually intrinsic reaction coordinates giving a lower activation energy (IRC-LAE), shown with a thick solid line in Fig. 5, exists as a path which connects the initial point (q_1=10.5 Å, q_2=0 Å) with the final point (q_1=8.85 Å, q_2=0.38 Å) in the reaction path by this calculation. However this model calculation indicates that such reaction coordinates are not selected in the polymerization under high-pressure. The IRC-EF and the IRC-LAE are reploted in Fig. 6, where the IRC-EF recalculated under a condition that the system is released from the external force at the place reached on the seam. The activation energy in the IRC-EF, defined to be the difference in energy between the the initial state and the seam, is found to be 4.15 eV, where the transition point is at q_1=8.58 Å, q_2=0.61 Å. When the IRC-LAE is selected, the value is 2.83 eV, with the transition point being at q_1=9.20 Å, q_2=0.15 Å..

The reaction coordinates during the experimental depolymerization are expected to be close to the IRC-LAE since no external force affects the system and only thermal vibration is a driving force of the reaction. Therefore, the IRC-LAE should be compared with the experimental result (Fig. 4). The energy difference between the two minima is estimated to be 0.85 eV, which is amaz-

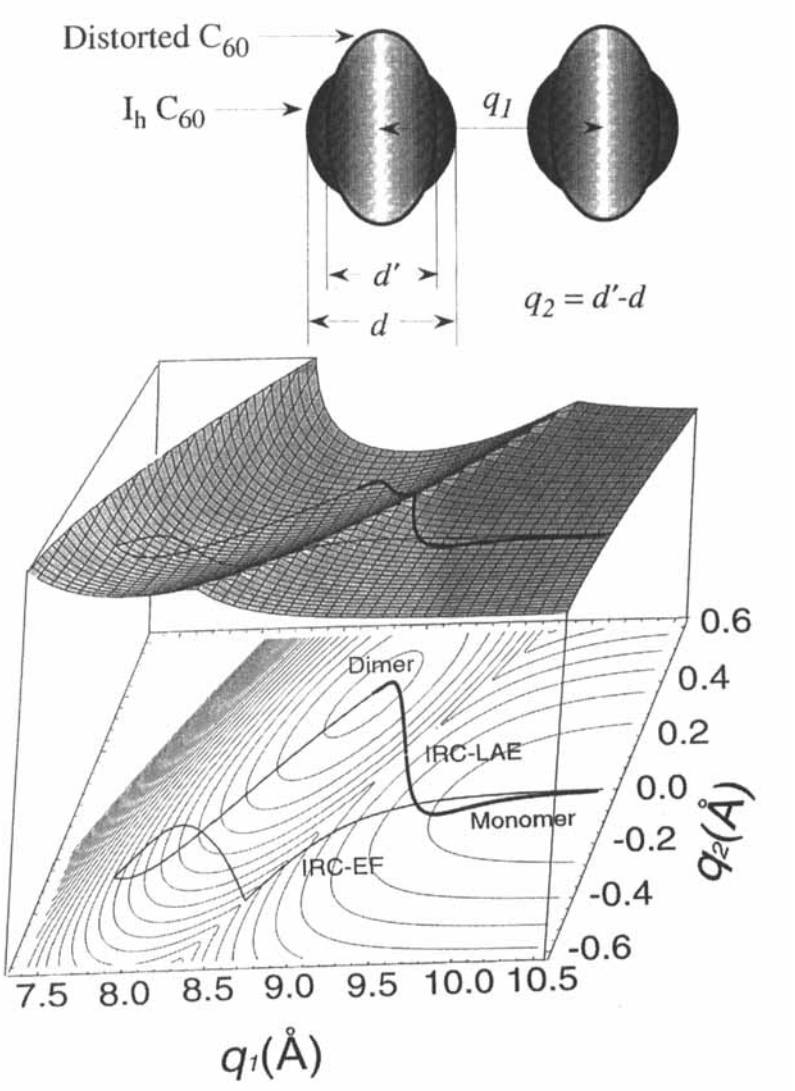

FIGURE 5 Potential energy maps of C_{60} dimer and the reaction coordinates of bond-formation and bond-breaking. The upper figure is a stereoscopicmap, the lower is a contour map. The thin and thick lines show the IRC-EF and IRC-LAE, respectively. The upper figure shows the definition of q_1 and q_2 coordinates

ingly close to the observed value 0.69 eV, indicating that the present calculation describes the stable states in a reasonable accuracy. The activation barrier 2.83 eV, on the other hand, is larger than the experimental result 1.75 eV [18]. Consid-

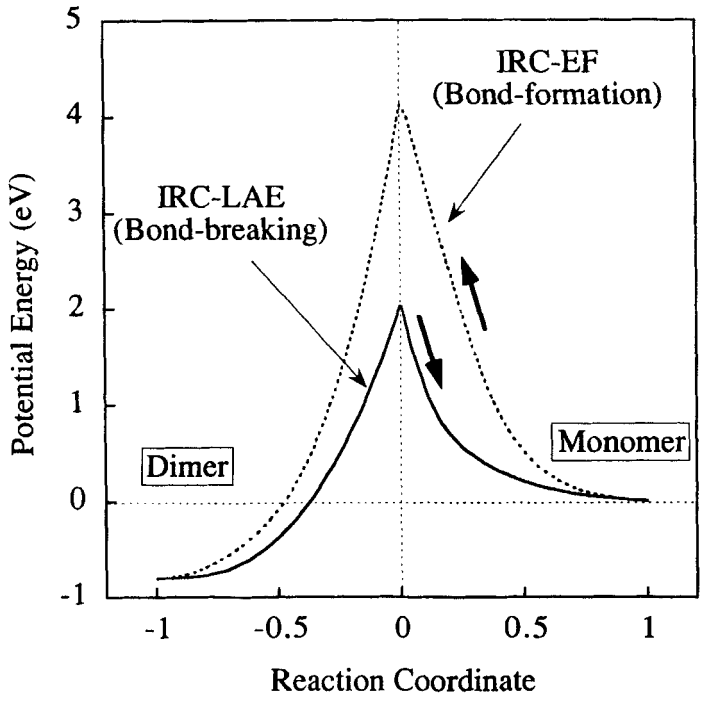

FIGURE 6 Activation barriers of bond-formation and bond-breaking in C_{60} dimer. The reaction coordinate is defined by normalizing with the length of reaction paths in Fig. 5. Reaction coordinate=0 is on the seam in Fig. 5

ering that the present calculation is comparable to 2.4 eV obtained by an LDA calculation [21], the present model is not sufficient for describing the region near the seam. Figure 6 reveals that the bond-breaking process has a smaller activation energy than the polymerization. This explains the reason why the polymerization requires harder experimental conditions than the depolymerization although the polymer phase is more stable than the monomer phase. In general, most of the experimental results are reasonably explained by the present calculation taking the deformation of molecules into account. This result indicates that the polymerization of C_{60} is chemically quite unique, since the internal degree of freedom in large fullerene molecules plays an important role in the energetics.

IV. CONCLUSION

We have investigated energetics and reaction paths for the polymerization of fullerenes. A calorimetry experiment revealed that the polymeric forms of C_{60} is

more stable than the monomeric form. The stabilization energy decreases with increasing the intermolecular [2+2] bonds. Combining the present and the dilatometry experiments, we have established an experimental potential curve for the dimerization. Moreover, we have performed a theoretical calculation of a energy contour map and determined the intrinsic reaction coordinates. The present calulation, taking the internal deformation of C_{60} into account, well explains for the drastic difference in experimental conditions for the polymerization and the depolymerization processes.

Acknowledgements

This work has been supported by a grant from the Japan Society for the Promotion of Science (RFTF96P00104, MPCR-363/96–03262), from the Grant-In-Aid for Scientific Research on the Priority Area "Fullerenes and Nanotubes" the Ministry of Education, Science, Sports, and Culture.

References

(1) E. Osawa, Kagaku (in Japanese) **25**, 854 (1970).
(2) H. W. Kroto, J. R. Heath, S. C. O'Brien, R. F. Curl and R. E. Smalley, Nature (London) **354**, 56 (1985).
(3) W. Krätchmer, L. C. Lamb, K. Fostiropoulos and D. R. Huffman, Nature (London) **347**, 354 (1990).
(4) R. C. Haddon, A. F. Hebard, M. J. Rosseinsky, D. W. Murphy, S. J. Duclos, K. B. Lyons, B. Miller, J. M. Rosamilla, R. M. Fleming, A. R. Kortan, S. H. Glarum, A. V. Makhija, A. J. Muller, R. H. Eick, S. M. Zahurak, R. Tycko, G. Dabbagh and F. A. Thiel, Nature (London) **350**, 320 (1991).
(5) A. F. Hebard, M. J. Rosseinsky, R. C. Haddon, D. W. Murphy, S. H. Glarum, T. T. M. Palstra, A. P. Ramirez, and A. R. Kortan, Nature (London) **350**, 600 (1991).
(6) A. M. Rao, P. Zhou, K.-A. Wang, G. T. Hager, J. M. Holden, Y. Wang, W.-T. Lee, X.-X. Bi, P. C. Eklund, D. S. Cornett, M. A. Duncan, and I. J. Amster, Science **259**, 955 (1993).
(7) O. Chauvet, G. Oszlányi, L. Forro, P. W. Stephens, M. Tegze, G. Faigel, and A. Jánossy, Phys. Rev. Lett. **72**, 2721 (1994).
(8) Y. Iwasa, T. Arima, R. M. Fleming, T. Siegrist, O. Zhou, R. C. Haddon, L. J. Rothberg, K. B. Lyons, H. L. Carter Jr., A. F. Hebard, R. Tycko, G. Dabbagh, J. J. Krajewski, G. A. Thomas, and T. Yagi, Sience **254**, 1570 (1994).
(9) M. Núñez-Regueiro, L. Marques, J.-L. Hodeau, O. Béthoux, and M. Perroux, Phys. Rev. Lett. **74**, 278 (1995).
(10) L. Marques, J.-L. Hodeau, M. Núñez-Regueiro, and M. Perroux, Phys. Rev. B**54**, R12633 (1996).
(11) V. Agafonov, V. A. Davydov, L. S. Kashevarova, A. V. Rakhmanina, A. Kahn-Harari, P. Dubois, R. Céolin, and H. Szwarc, Chem. Phys. Lett. **267**, 193 (1997).
(12) R. Moret, P. Launois, P.-A. Persson, and B. Sundqvist, Europhys. Lett. **40**, 55 (1997).
(13) G.-W. Wang, K. Komatsu, Y. Murata, and M. Shiro, Nature **387**, 583 (1997).
(14) Y. Iwasa, K. Tanoue, T. Mitani, A. Izuoka, T. Sugawara, and T. Yagi, Chem. Comm. 1411 (1998).
(15) K. Kamaras, Y. Iwasa, and L. Forro, Phys. Rev. B**55**, 10999 (1997).
(16) V. C. Long, J. L. Musfeldt, K. Kamaras, Y. Iwasa, and W. E. Mayo, Ferroelectrics, in press.
(17) Y. Iwasa, K. Tanoue, T. Mitani, and T. Yagi, Phys. Rev. B**58**, 16374 (1998).
(18) P. Nagel, V. Pasler, S. Lebedkin, C. Meingast, B. Sundqvist T. Tanaka, and K. Komatsu, *Progress in Molecular Nanostructures*, edited by H. Kuzmany, J. Fink, M. Mehring, and S. Roth (American Institute of Physics, New York, 1998), pp. 194.

(19) T. Ozaki, Y. Iwasa, and T. Mitani, Chem. Phys. Lett. **285**, 289 (1998).
(20) K. Fukui, S. Kato and H. Fujimoto, J. Am. Chem. Soc. **97**, 1 (1975).
(21) G. B. Adams, J. B. Page, O.F. Sankey and M. O'Keeffe, Phys. Rev. B**50**, 17471 (1994).